AIAA JOURNAL
Vol. 48, No. 8, August 2010

Vibration of Plate with Curvilinear Stiffeners Using Mesh-Free Method

Ali Yeilaghi Tamijani* and Rakesh K. Kapania†
Virginia Polytechnic Institute and State University, Blacksburg, Virginia 24061

DOI: 10.2514/1.43082

The element-free Galerkin method, which is based on the moving-least-squares approximation, is developed for vibration analysis of unitized structures (e.g., a plate with curvilinear stiffeners). The plate and stiffeners are modeled using the first-order shear deformation theory and Timoshenko beam theory, respectively. The moving-least-squares approximation does not satisfy the delta function property. Consequently, an approximation method (e.g., the well-known penalty method) must be used for imposing essential boundary conditions. A key benefit of using element-free Galerkin for the vibration analysis of a stiffened panel is that the locations and curvatures of the stiffeners can be changed without modifying the plate nodes. Numerical results for different stiffeners, configurations, and boundary conditions are presented. All results are verified using the commercial finite-element software ANSYS. Excellent agreement is seen in all cases. A comparison of the present formulations with other available results for stiffened plates is also made. The mesh-free approach yields highly accurate results for the plates with curvilinear stiffeners.

Nomenclature

A	=	area
a_R	=	Rayleigh damping coefficient
b	=	stiffener binormal direction
b_R	=	Rayleigh damping coefficient
b_s	=	stiffener width
C	=	damping
D_p	=	plate stress–strain matrix for an isotropic material
D_s	=	stiffener stress–strain matrix for an isotropic material
$\det J$	=	Jacobian of the transformation
E	=	elastic modulus
F	=	force vector
h_p	=	plate thickness
h_s	=	stiffener thickness
I	=	second moment of stiffener cross-sectional area
J	=	L_2 norm
J_t	=	torsional stiffness of stiffener
K	=	stiffness matrix
K_G	=	shear correction factor
L	=	Lagrangian
ℓ	=	stiffener domain
M	=	mass matrix
m	=	mass
N_i	=	shape function
n	=	stiffener normal direction
p	=	plate
$p(X)$	=	monomial basis
r_i	=	support size
S	=	centroidal distance of stiffener to plate midsurface
s	=	stiffener
T_p	=	plate kinetic energy
T_s	=	stiffener kinetic energy
T_{sp}	=	transformation matrix relating stiffener nodal displacements and plate nodal displacements
t	=	stiffener tangential direction
t_1, t_2	=	arbitrary time limits
U_p	=	plate strain energy
U_s	=	stiffener strain energy
u	=	displacement
$\bar{u}$	=	prescribed displacement
u_i	=	nodal displacements
u_{p0}	=	plate displacement along x direction
u_{s0}	=	stiffener displacement along x direction
v_{p0}	=	plate displacement along y direction
v_{s0}	=	stiffener displacement along y direction
w	=	weight function
w_{p0}	=	plate displacement along z direction
w_{s0}	=	stiffener displacement along z direction
α	=	angle between stiffener tangential direction (t) and x axis
α_p	=	penalty parameter
Γ_t	=	prescribed tractions boundary
Γ_u	=	prescribed displacements boundary
ε_p	=	plate strain vector
ε_s	=	stiffener strain vector
ζ	=	natural coordinate
θ_n	=	stiffener rotation with respect to t direction
θ_t	=	stiffener rotation with respect to n direction
Λ	=	coordinate transformation matrix
ρ	=	density
υ	=	Poisson's ratio
φ_{px}	=	plate rotation with respect to y axis
φ_{py}	=	plate rotation with respect to x axis
φ_{sx}	=	stiffener rotation with respect to y axis
φ_{sy}	=	stiffener rotation with respect to x axis
Ω	=	plate domain
$1/R$	=	curvature

Presented as Paper 2009-2647 at the 50th AIAA/ASME/ASCE/AHS/ASC Structures, Structural Dynamics, and Materials Conference, Palm Springs, CA, 4–7 May 2009; received 5 January 2009; revision received 4 October 2009; accepted for publication 30 October 2009.

*Ph.D. Candidate, Department of Engineering Science and Mechanics; ayt@vt.edu. Member AIAA.

†Mitchell Professor, Department of Aerospace and Ocean Engineering; rkapania@vt.edu. Associate Fellow AIAA.

I. Introduction

STIFFENED plate or shell structures have wide applications in the industry. These structures usually consist of a base structure and local reinforcement elements called stiffeners to improve the static and dynamic characteristics of the base structure. An economical design is achieved through a proper selection of the plate and the stiffener sizes while reducing the overall panel weight.

A number of analytical and numerical models for the analysis of the stiffened plates have been reported in the literature. Earlier researchers simulated stiffened plates with grillage models [1] or orthotropic models [2]. A more accurate model is achieved by representing the plate and stiffeners separately and imposing appropriate continuity between them. Olsen and Hazell [3] presented a theoretical and experimental comparison study on the vibrations of stiffened plates. The finite-element method (FEM) and a real-time laser holography were used for the theoretical predictions and the experimental verifications, respectively.

Bhimaraddi et al. [4] developed a FEM for the analysis of orthogonally stiffened shells of revolution. They used shell and curved beam elements in their model. These two elements were isoparametric elements in which the effects of shear deformation and rotary inertia effects were taken into account. A FEM was introduced for the free-vibration analysis of stiffened plates by Holopainen [5]. The main advantage of this plate-bending element, as compared to the other FEMs, is that this element is free from shear locking. The Ritz–Galerkin method was used for solving free vibration of the stiffened plate by Chen et al. [6], with B-splines as the trial functions. In their research, the spline compound strip method was used. The spline compound strip method can be considered as a special form of the FEM.

The differential quadrature (DQ) method was studied by Zeng and Bert [7], and it was extended to study the free vibration of eccentrically stiffened plates. Gangadhara Prusty and Satsangi [8] presented static analysis of stiffened shells. The shell is analyzed using an eight-noded isoparametric element, and the stiffener element is considered as a three-noded isoparametric curved-beam element, and the stiffness matrix is calculated using the standard principles of finite-element analysis. Also, a new four-noded stiffened plate-bending element was proposed by Barik and Mukhopadhyay [9] for the analysis of both unstiffened and stiffened plates. This element was derived by combining the four-noded rectangular plane stress element, having 8 degrees of freedom, with the simplest rectangular plate-bending element, having 12 degrees of freedom. One of the advantages of their approach is that the orientation and the position of the stiffeners inside the plate element are without any restriction and, hence, need not necessarily be positioned between nodes.

As it has been mentioned earlier, many methodologies have been implemented for various free-vibration stiffened plate problems. These methods include analytical and numerical techniques, such as the Ritz method, the DQ method, the finite strip method, and the FEM.

In recent decades, meshless methods have attracted much attention because of the need for no elements for interpolation purposes. Belytschko et al. [10] developed the element-free Galerkin (EFG) method and used it to model the elasticity and heat conduction problems. The moving-least-squares (MLS) method is used to construct the shape function. Belytschko et al. introduced a background cell structure to find integration by numerical quadrature, and Lagrange multipliers are used to enforce essential boundary conditions.

Krysl and Belytschko [11] developed a meshless approach for the analysis of the arbitrary Kirchhoff shells by the EFG method. The equations are based on the geometrically exact theory of shear flexible shells. The method is based on MLS approximation. The EFG method is almost identical to the conventional FEM, as both of them are based on the Galerkin formulation and employ local interpolation to approximate the trial functions. The key differences are in the interpolation methods, the integration schemes, and in the enforcement of essential boundary conditions. Belytschko et al. [12] also studied different features of the kernel methods, the MLS methods, and the partition of the unity methods. It was shown that these methods can have similar features, especially the MLS method: if certain conditions are imposed, the MLS method can be similar to the kernel method. Two kinds of meshless methods, collocation methods, and Galerkin methods were also considered by using the MLS and partition of unity methods, and convergence of these methods for various structures was studied.

Peng et al. [13,14] used the EFG method for the static and dynamic analysis of plate with straight stiffeners in the x and y directions. It has been shown in their paper that, by using the EFG method, they avoid the need for remeshing that occurs with the FEM, because the stiffeners need to be placed along the mesh lines, and the change of the stiffener position leads to remeshing of the entire plate domain.

One of the main issues in numerical analysis is the CPU time, and it is obvious that remeshing (e.g., in shape optimization) will increase it. Bobaru and Mukherjee [15] studied the shape optimization of the fillet using the EFG method, and the results were compared to the FEM, the boundary-element method (BEM), and the boundary-counter method. They showed that the cost of remeshing, which is required in many shape optimizations using FEM or BEM, can be eliminated by using the EFG method.

In this research, an EFG method for the vibration analysis of a stiffened plate, based on the use of MLS, is demonstrated. The EFG method employs the MLS approximants to approximate the trial functions. One of the problems with the MLS approximants is that, in general, they do not pass through the data used to fit the curve. Therefore, the essential boundary conditions in the EFG methods cannot be easily and directly enforced. Several approaches have been studied for enforcing the essential boundary conditions in the EFG method, such as the direct collocation method, the Lagrange multipliers method, and the penalty method. The essential boundary conditions in the present formulation are imposed by the penalty method. Although, in EFG method, there is no need of mesh to construct the shape function; in order to compute the integrals in the weak form, a background cell is required.

By using EFG, the natural frequencies, the natural modes, and the frequency response are calculated for stiffened panels. The determination of natural frequencies, natural modes, and the frequency response of a plate with curvilinear stiffeners using the meshless method, to the authors' knowledge, has not previously appeared. The plate is assumed to be of uniform thickness and with arbitrary boundaries on the edges. The plate and stiffeners are modeled using the first-order shear deformation theory and the Timoshenko beam theory, respectively. Eccentricity of the stiffeners is included in the formulation. The stiffener cross section is assumed to be symmetric about the stiffener binormal axis, and the stiffener is assumed to remain perpendicular to the plate during deformation. The main advantage of this formulation is that the stiffeners can be placed anywhere within the plate, and they do not necessarily follow the nodal plate lines. The meshless methods may thus have a great value during the optimal design of stiffened panels with curvilinear stiffeners, which will require a large number of mesh generations if the regular finite element is used.

In the following sections, first, the meshless method for analyzing vibration analysis of a stiffened plate is developed. A number of numerical examples are given to reveal the behavior of the meshless method for various stiffened panels. The results obtained by the present approach are compared to those either theoretically or experimentally available. Also, the meshless results are compared to those obtained using the ANSYS, commercially available, finite-element software. A good comparison between the two sets of results is seen. The present formulation can thus be used for studying vibration of unitized structures with curvilinear stiffeners.

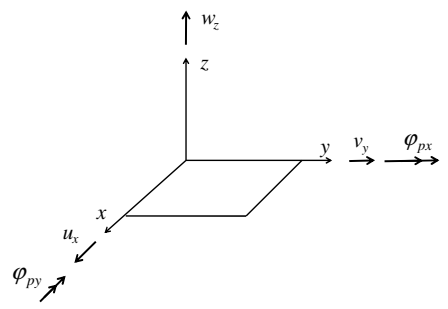

Fig. 1 Directions of the generalized displacements of the plate.

II. Formulation of the Problem

A. Strain and Kinetic Energies of the Plate and Stiffener

The strain and kinetic energies of the plate can be written as [16]

$$U_p = \frac{1}{2}\int_A \varepsilon_p^T D_p \varepsilon_p \, \mathrm{d}A; \qquad T_p = \frac{1}{2}\int_A \dot{u}_p^T m_p \dot{u}_p \, \mathrm{d}A \tag{1}$$

where the dot represents the differentiation with respect to time. D_p, ε_p, m_p, and u_p are defined in the Appendix. The degrees of freedom of the plate are shown in Fig. 1.

Line Γ in a three-dimensional global coordinate system x, y, and z is shown in Fig. 2. The local coordinates are t, n, and b in tangential, normal, and binormal directions, respectively. R is the radius of curvature, and the curvature is in the x-y plane; consequently, b is in z direction. The angle between the t and x axes is α. The line Γ can be defined by

$$x = x(\zeta) \qquad y = y(\zeta) \tag{2}$$

in which x and y are global coordinates, and ζ is the natural coordinate for parameterizing the curve, as seen in Fig. 3. The $\det J$ may be defined as [17]

$$\det J = \sqrt{\left(\frac{\mathrm{d}x}{\mathrm{d}\zeta}\right)^2 + \left(\frac{\mathrm{d}y}{\mathrm{d}\zeta}\right)^2} \tag{3}$$

The curvature is [17]

$$\frac{1}{R} = \left(\frac{\mathrm{d}x}{\mathrm{d}\zeta}\frac{\mathrm{d}^2y}{\mathrm{d}\zeta^2} - \frac{\mathrm{d}y}{\mathrm{d}\zeta}\frac{\mathrm{d}^2x}{\mathrm{d}\zeta^2}\right)\Big/ (\det J)^3 \tag{4}$$

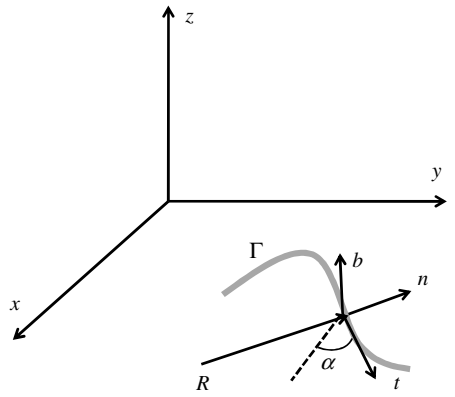

Fig. 2 Local and global coordinate systems for curvilinear stiffener.

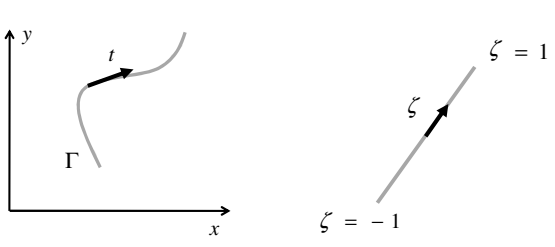

a) **b)**

Fig. 3 Plots of a) curved stiffener in x-y plane and b) its transformed plane.

The strain vector can be written as [17]

$$\varepsilon_s = \begin{Bmatrix} \varepsilon_t \\ \gamma_b \\ \gamma_n \\ \kappa_t \\ \kappa_n \end{Bmatrix} = \begin{bmatrix} \frac{1}{\det J}\frac{\mathrm{d}}{\mathrm{d}\zeta} & \frac{1}{R} & 0 & 0 & 0 \\ -\frac{1}{R} & \frac{1}{\det J}\frac{\mathrm{d}}{\mathrm{d}\zeta} & 0 & 0 & 0 \\ 0 & 0 & 1 & 0 & \frac{1}{\det J}\frac{\mathrm{d}}{\mathrm{d}\zeta} \\ 0 & 0 & \frac{1}{\det J}\frac{\mathrm{d}}{\mathrm{d}\zeta} & \frac{1}{R} & 0 \\ 0 & 0 & -\frac{1}{R} & \frac{1}{\det J}\frac{\mathrm{d}}{\mathrm{d}\zeta} & 0 \end{bmatrix} \begin{Bmatrix} u_t \\ v_n \\ \theta_t \\ \theta_n \\ w_b \end{Bmatrix} = L_s u_s' \tag{5}$$

where u_t, v_n, and w_b are the reference plane (which, in this paper, is placed in the midplane of the plate) displacements along the t, n, and b directions, respectively, and θ_t and θ_n are the rotations with respect to the n and t axes (Fig. 4). The displacement fields, in terms of the global coordinate system, are (Fig. 2)

$$u_s' = \begin{Bmatrix} u_t \\ v_n \\ \theta_t \\ \theta_n \\ w_s \end{Bmatrix} = \begin{bmatrix} \cos\alpha & \sin\alpha & 0 & 0 & 0 \\ -\sin\alpha & \cos\alpha & 0 & 0 & 0 \\ 0 & 0 & \cos\alpha & \sin\alpha & 0 \\ 0 & 0 & -\sin\alpha & \cos\alpha & 0 \\ 0 & 0 & 0 & 0 & 1 \end{bmatrix} \begin{Bmatrix} u_{s_0} \\ v_{s_0} \\ \varphi_{sx} \\ \varphi_{sy} \\ w_{s_0} \end{Bmatrix} = \Lambda u_s \tag{6}$$

where u_{s_0}, v_{s_0}, and w_{s_0} are the reference plane displacements along the x, y, and z directions, respectively, and φ_{sx} and φ_{sy} are the rotations with respect to the y and x axes. By using Eq. (5), the strain in global coordinate system can be written as

$$\varepsilon_s = L_s \Lambda u_s \tag{7}$$

The matrix L_s is defined by Eq. (5). The strain energy can be defined as [17]

$$U_s = \frac{1}{2}\int_{-1}^{1} \varepsilon_s^T D_s \varepsilon_s \det J \, \mathrm{d}\zeta \tag{8}$$

where the generalized stiffener stress–strain matrix for an isotropic material is

$$D_s = \begin{bmatrix} E_s A_s & 0 & 0 & E_s A_s \bar{S} & 0 \\ 0 & G_s A_n & 0 & 0 & G_s A_s \bar{S} \\ 0 & 0 & G_s A_b & 0 & 0 \\ E_s A_s \bar{S} & 0 & 0 & E_s I_n & 0 \\ 0 & G_s A_s \bar{S} & 0 & 0 & G_s J_t \end{bmatrix} \tag{9}$$

In Eq. (9), E_s is Young's modulus; G_s is Shear's modulus; $A_s = b_s h_s$, where b_s and h_s are the width and height of stiffener, is the stiffeners's cross-sectional area; $\bar{S}$ is the centroidal distance of the stiffener to the plate at midsurface; $A_n = k_n A_s$ and $A_b = k_b A_s$, where k_n and k_b are the shear correction factors [17], are the shear areas; I_n is the second moment of the stiffener cross-sectional area about the n axis; and J_t is torsional constant of stiffener, which an approximate $J_t \approx \frac{1}{3} h_s b_s^3$ is used. For the concentric stiffener and the eccentric

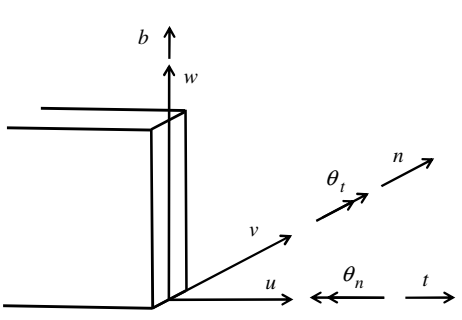

Fig. 4 Directions of the generalized displacements of the stiffener.

stiffener, we have $\bar{S}=0$, $I_n=\frac{1}{12}b_s h_s^3$, and $\bar{S}=(h_p/2)+(h_s/2)$ and $I_n=\frac{1}{12}b_s h_s^3+A_s\bar{S}^2$, respectively. The kinetic energy can be written as

$$T_s=\frac{1}{2}\int_{-1}^{1}(\Lambda\dot{u}_s)^T m_s(\Lambda\dot{u}_s)\det J\,\mathrm{d}\zeta \tag{10}$$

where

$$m_s=\rho_s\begin{bmatrix} A_s & 0 & A_s\bar{S} & 0 & 0\\ 0 & A_s & 0 & A_s\bar{S} & 0\\ A_s\bar{S} & 0 & I_n & 0 & 0\\ 0 & A_s\bar{S} & 0 & I_n+I_t & 0\\ 0 & 0 & 0 & 0 & A_s\end{bmatrix} \tag{11}$$

where ρ_s is the density of stiffener material, and I_t is the second moment of the stiffener cross-sectional area about the t axis.

B. Description of the Moving-Least-Squares Approximation

In the following section, we provide a brief description of the MLS approximation and introduce the notation and some definitions (see [18] for the details). Consider a subdomain Ω_x, the neighborhood of a point X, denoted as the domain of definition of the MLS approximation for the trial function at X, which is located in the problem domain Ω. To approximate the distribution of function u in Ω_x over a number of local nodes, the MLS approximant $u^h(X)$ of u, $\forall\, x\in\Omega_x$ can be defined by

$$u^h(X)=p^T(X)a(X)\quad\forall\ x\in\Omega_x \tag{12}$$

where $p^T(X)=[p^1(X)\cdots p^m(X)]$ is a complete monomial basis of order m, and $a(X)$ is a vector containing coefficients $a_j(X)$, which are functions of the space coordinates $X=[x,y]$. In this paper, the quadratic basis $p^T=[1,x,x^2]$ is one-dimensional (1-D), $m=3$, $p^T=[1,x,y,x^2,xy,y^2]$ is two-dimensional, and $m=6$ is used.

The unknown coefficients $a_j(X)$ are obtained by the minimization of a weighted discrete L_2 norm:

$$J(X)=\sum_{i=1}^{n}w(X_i)[p^T(X_i)a(X)-\hat{u}_i]^2 \tag{13}$$

where $w(X_i)$ is the weight function that is associated with node i, $w(X_i)=0$ outside Ω_x, n is the number of nodes in Ω_x, and $\hat{u}_i$ are the nodal parameters. In this research, the spline weight function is used:

$$w(X_i)=\begin{cases}1\text{–}6\left(\frac{d_i}{r_i}\right)^2+8\left(\frac{d_i}{r_i}\right)^3-3\left(\frac{d_i}{r_i}\right)^4 & 0\le d_i<r_i\\ 0 & d_i\ge r_i\end{cases};\qquad d_i=|X-X_i| \tag{14}$$

where r_i is the size of the support for the weight function $w(X_i)$, and it determines the size of the support for node X_i. If the domain of influence is a circle, r_i is the radius of the circle. If the domain of influence is rectangular, the weight function can be written in tensor product form as $w(X_i)=w(x_i)w(y_i)$, [12] and r_i can be dx_i and dy_i, the lengths of the rectangular support in the x and y directions (see Fig. 5). The minimization of $J(x)$ in Eq. (13), with respect to $a(X)$, leads to the following system of linear equations for the determination of $a(X)$:

$$A(X)a(X)=B(X)\hat{u} \tag{15}$$

where

$$A(X)=\sum_{i=1}^{n}w(X_i)p(X_i)p^T(X_i)$$
$$B(X)=[\,w(X_1)p(X_1)\quad\cdots\quad w(X_n)p(X_n)\,] \tag{16}$$

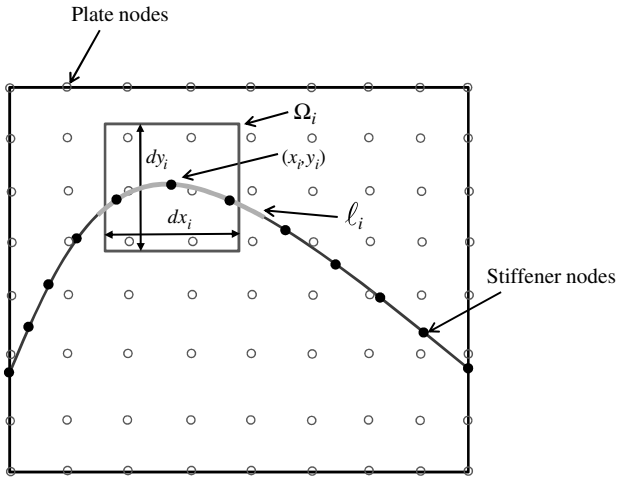

Fig. 5 Plate and stiffener nodes for a plate with a curvilinear stiffener.

By substituting Eq. (15) into Eq. (12),

$$u^h=\sum_{i=1}^{n}N_i(X)\hat{u}_i \tag{17}$$

where the shape function $N_i(X)$ is defined as

$$N_i(X)=\sum_{j=1}^{m}p_j(X)[A^{-1}(X)B(X)]_{ji} \tag{18}$$

C. Discrete Equations of the Element-Free Galerkin Method

To obtain the discrete equations of the EFG method, the equations are rewritten by using the MLS basis function. As seen in Fig. 5, the supports of the weights for the plate's nodes and the stiffener's nodes are rectangular (Ω_i) and spline (ℓ_i), respectively. The lengths of the rectangular support in the x and y directions are dx_i and dy_i. By using the shape function that has been introduced in Eq. (18), u_p and u_s, the plate and stiffener displacements vector, respectively, can be prescribed as

$$u_p=N_p\delta_p;\qquad u_s=N_s\delta_s \tag{19}$$

where N_p and N_s are the shape functions [Eq. (18)] related to the plate and stiffener, respectively. Also, δ_p and δ_s are given in the Appendix. Substituting Eq. (19) into Eqs. (A2) and (7) results in

$$\varepsilon_p=B_p\delta_p;\qquad \varepsilon_s=B_s\Lambda\delta_s \tag{20}$$

where B_p and B_s are defined in the Appendix.

D. Transformation Equations

Two approaches, to the authors' knowledge, for employing the displacement compatibility conditions at the contact surface between the plate and the stiffener have been reported in the literature. In the first approach [19], the reference axis of the stiffener is considered on the neutral axis of the stiffener, and the stress–strain matrix [Eq. (9)] is calculated based on this assumption. By using this approach $\bar{S}$, the distance between the neutral axis of the plate to the neutral axis of the stiffener, as seen in Fig. 6, can change the transformation matrix, which transforms the node parameters of the stiffener to the node parameters of the plate. In the second approach [8], which is used in the current research, the reference plane of the stiffener is placed in the midplane of the plate. Consider node i of the stiffener located at (x_i, y_i) (see Fig. 5). For this node, the displacement compatibility at the contact surface between the plate and the stiffener impose, such that,

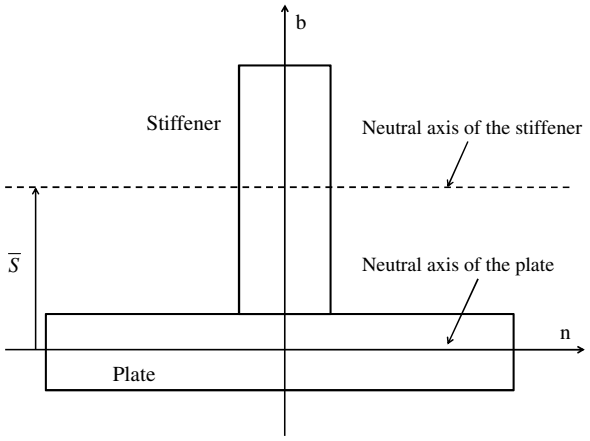

Fig. 6 Cross section of plate and stiffener.

$$u_p(x_i, y_i, z)|_{z=h_p/2} = u_s(x_i, y_i, z)|_{z=h_p/2};$$
$$v_p(x_i, y_i, z)|_{z=h_p/2} = v_s(x_i, y_i, z)|_{z=h_p/2};$$
$$w_{p_0}(x_i, y_i) = w_{s_0}(x_i, y_i) \tag{21}$$

By using Eq. (A1), Eq. (21) can be written as

$$u_{p_0}(x_i, y_i) = u_{s_0}(x_i, y_i); \qquad v_{p_0}(x_i, y_i) = v_{s_0}(x_i, y_i);$$
$$w_{p_0}(w_i, y_i) = w_{s_0}(x_i, y_i); \qquad \varphi_{px}(x_i, y_i) = \varphi_{sx}(x_i, y_i);$$
$$\varphi_{py}(x_i, y_i) = \varphi_{sy}(x_i, y_i) \tag{22}$$

The square domain related to this node is $\mathbf{\Omega}_i$, which includes the plate's n nodes. The 1-D domain related to this node is ℓ_i, which contains the stiffeners' N nodes. The domain and nodes are shown in Fig. 5. By using the discrete equations and the shape functions that have been introduced in Eq. (19), Eq. (22) is rewritten as

$$\sum_{I=1}^{n} N_{pI}(x_i, y_i)\delta_{puI} = \sum_{J=1}^{N} N_{sJ}(x_i, y_i)\delta_{suJ}; \qquad I = 1, \ \ldots, n;$$
$$\sum_{I=1}^{n} N_{pI}(x_i, y_i)\delta_{pvI} = \sum_{J=1}^{N} N_{sJ}(x_i, y_i)\delta_{svJ}; \qquad J = 1, \ \ldots, N;$$
$$\sum_{I=1}^{n} N_{pI}(x_i, y_i)\delta_{pwI} = \sum_{J=1}^{N} N_{sJ}(x_i, y_i)\delta_{swJ};$$
$$\sum_{I=1}^{n} N_{pI}(x_i, y_i)\delta_{p\varphi xI} = \sum_{J=1}^{N} N_{sJ}(x_i, y_i)\delta_{s\varphi xJ};$$
$$\sum_{I=1}^{n} N_{pI}(x_i, y_i)\delta_{p\varphi yI} = \sum_{J=1}^{N} N_{sJ}(x_i, y_i)\delta_{s\varphi yJ} \tag{23}$$

Rewriting Eq. (23) in matrix form,

$$T_{su}\delta_{su} = T_{pu}\delta_{pu}; \qquad T_{sv}\delta_{sv} = T_{pv}\delta_{pv}; \qquad T_{sw}\delta_{sw} = T_{pw}\delta_{pw};$$
$$T_{s\varphi x}\delta_{s\varphi x} = T_{p\varphi x}\delta_{p\varphi x}; \qquad T_{s\varphi y}\delta_{s\varphi y} = T_{p\varphi y}\delta_{p\varphi y} \tag{24}$$

The T matrices are shown in the Appendix. From Eq. (24), we get

$$\delta_{su} = T_{su}^{-1}T_{pu}\delta_{pu}; \qquad \delta_{sv} = T_{sv}^{-1}T_{pv}\delta_{pv}; \qquad \delta_{sw} = T_{sw}^{-1}T_{pw}\delta_{pw};$$
$$\delta_{s\varphi x} = T_{s\varphi x}^{-1}T_{p\varphi x}\delta_{p\varphi x}; \qquad \delta_{s\varphi y} = T_{s\varphi y}^{-1}T_{p\varphi y}\delta_{p\varphi y} \tag{25}$$

All the nodal displacement ($\delta_{su}, \delta_{pu}, \ldots$) vectors for the stiffener and for the plate can be written in one vector, respectively. The transformation matrix relating the stiffener nodal displacements and the plate nodal displacements can be defined as

$$\delta_s = T_{sp}\delta_p \tag{26}$$

in which T_{sp} is the $5N \times 5n$ matrix, which transforms the node parameters of the stiffener to the node parameters of the plate.

E. Enforcement of Essential Boundary Conditions

As in the standard FEM, the EFG method uses the weak form of the problem to describe the equations of motion. The essential boundary conditions are accounted for by means of a penalty method. By using the principle of minimum potential energy, the Lagrangian can be defined as [20]

$$L = T_p + T_s - U_p - U_s + \int_{\Gamma_t} u^T f \, d\Gamma$$
$$-\frac{\alpha_p}{2}\int_{\Gamma_u} (u - \bar{u})^T (u - \bar{u}) \, d\Gamma \tag{27}$$

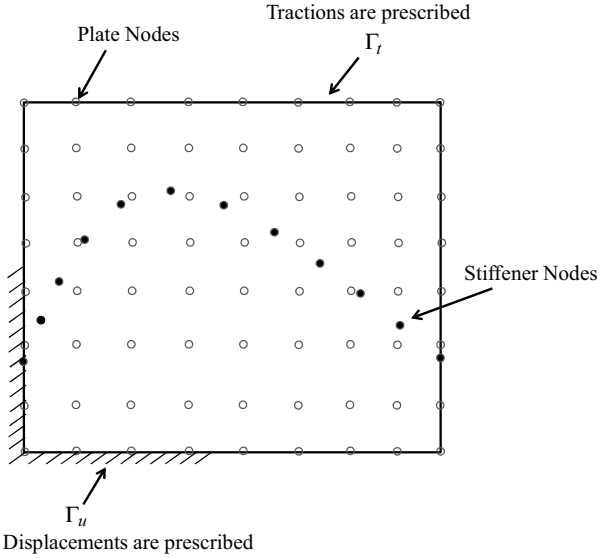

Fig. 7 Prescribed boundaries of the plate with a curvilinear stiffener.

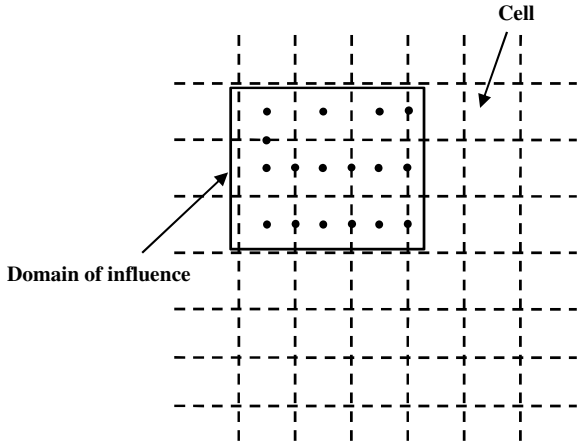

Fig. 8 Domain of influence and background cell structures.

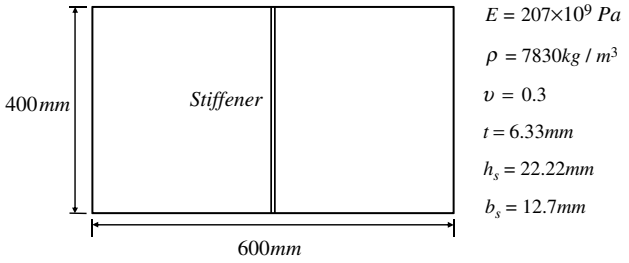

Fig. 9 Stiffened plate with single stiffener.

Table 1 Ten natural frequencies (Hz) for simply supported plate with single stiffener

Mode	Ritz (B-splines) [6]	FEM [4]	DQ [7]	ANSYS	Mesh-free
1	245	247	252	251	247
2	277	274	275	273	273
3	511	513	523	512	506
4	——	——	——	559	557
5	——	——	——	575	565
6	——	——	——	778	777
7	——	——	——	1028	1014
8	——	——	——	1039	1018
9	——	——	——	1060	1036
10	——	——	——	1094	1081

The boundary conditions are shown in Fig. 7. The prescribed displacement and traction on the boundaries are $\bar{u}$ and f.

An important consideration for using the penalty method is the choice of an appropriate penalty parameter α_p. We should note that the penalty terms will not only affect the diagonal entries of the system stiffness matrix but also the offdiagonal entries of the system matrix. The system stiffness matrix may become ill-conditioned when the offdiagonal entries are multiplied by a very large number. Hence, the main issue in using the penalty method is the proper choosing of the penalty parameter. From the literature review [20], the penalty parameter α_p can be chosen as $(10^3 - 10^7) \times E$, where E is the Young's modulus of the material under consideration.

F. Derivation of the Stiffness and Mass Matrices and the Force Vector

In the formulation of the linear EFG method, it is assumed that deformations remain small so that linear relations can be used to represent the strain as a function of the displacements in a body. The emphasis of the present work is on developing a formulation for the vibration analysis of the stiffened plates. Strain and kinetic energy expressions were derived. Then, by using transformation equation (26), they transform the node parameters of the stiffener to the node parameters of the plate by considering their positions within the plate. Consequently, the displacements are expressed only in terms of the plate nodes' degrees of freedom. In implementing the EFG method, the basis function was first defined. As was mentioned, in this research, the MLS basis function is used. The size of support for the weight function should be large enough to provide a sufficient number of nodes in the domain of definition of the MLS to warrant a reasonable accuracy. As has been reported by Zhu and Atluri [20], while using the MLS basis, the shape functions and their derivatives become strongly nonpolynomial. Consequently, the Gauss quadrature method in such a case may give a relatively large error. After finding the basis function and defining the shape function by considering the nodes, the background cell, as seen in Fig. 8, should be defined for integration. It should be noted that the background cells are independent of the structure's nodes and domain of influence. From the previous discussion, it is clear that the EFG method does not need elements, but it does need a cell structure to evaluate integrals.

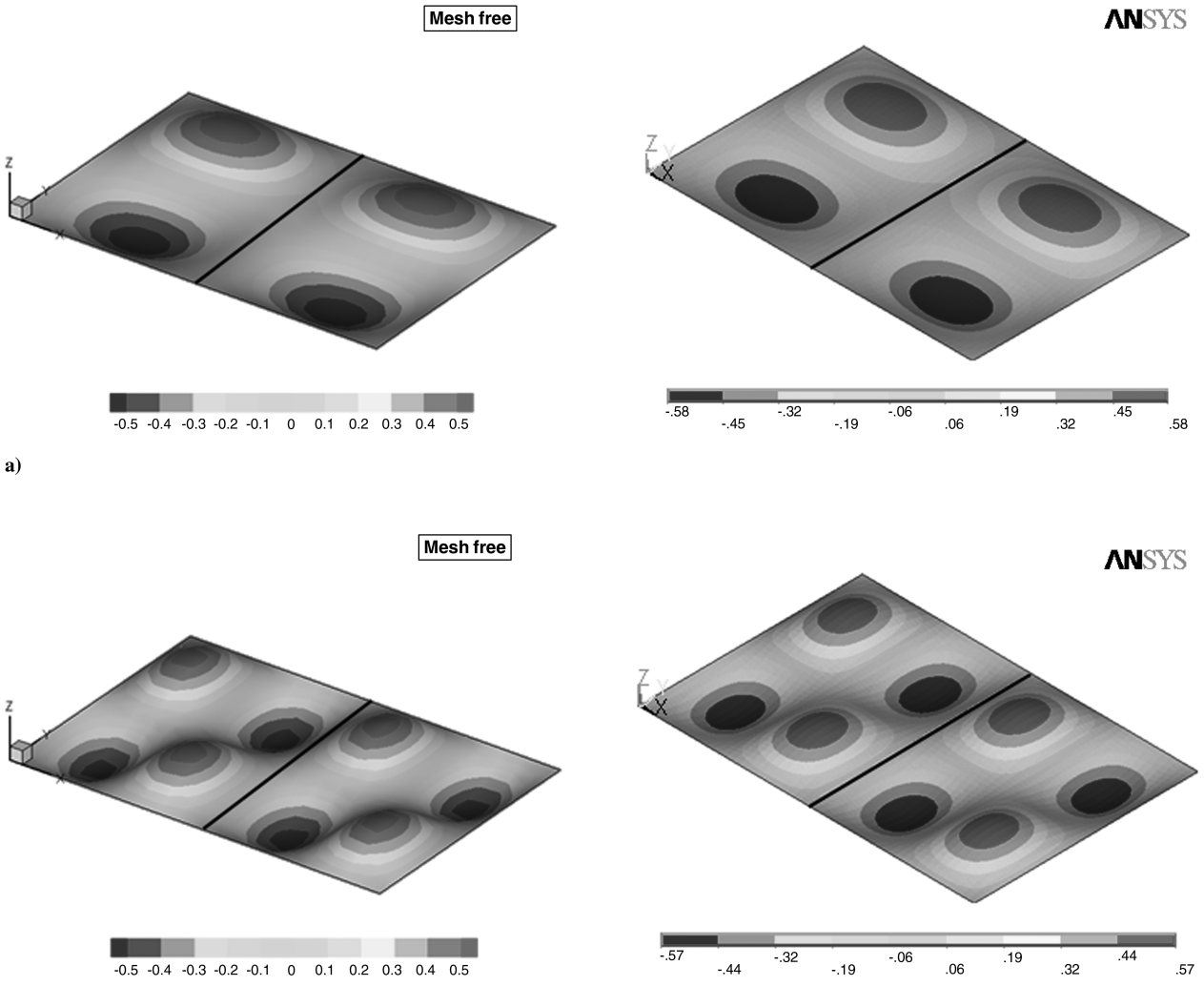

Fig. 10 Mode shapes obtained for a stiffened plate using a mesh-free method (left) and ANSYS (right): a) fifth mode shape and b) tenth mode shape.

By substituting Eqs. (19) and (20) into Eq. (1),

$$U_p = \frac{1}{2}\delta_p^T \int_A B_p^T D_p B_p \, \mathrm{d}A \delta_p; \qquad T_p = \frac{1}{2}\dot{\delta}_p^T \int_A N_p^T m_p N_p \, \mathrm{d}A \dot{\delta}_p \tag{28}$$

Also, first transform the displacements of the stiffener to the displacements of the plate by substituting Eq. (26) into Eqs. (19) and (20) and then substituting the results into the Eqs. (8) and (10):

$$U_s = \frac{1}{2}\delta_p^T T_{sp}^T \int_{-1}^{1} \Lambda^T B_s^T D_s B_s \Lambda \det J \, \mathrm{d}\zeta T_{sp} \delta_p;$$
$$T_s = \frac{1}{2}\dot{\delta}_p^T T_{sp}^T \int_{-1}^{1} \Lambda^T N_s^T m_s N_s \Lambda \det J \, \mathrm{d}\zeta T_{sp} \dot{\delta}_p \tag{29}$$

According to Hamilton's principle,

$$\delta \int_{t_1}^{t_2} L \, \mathrm{d}t = 0 \tag{30}$$

where L is the Lagrangian function of the stiffened plate, and t_1 and t_2 are the arbitrary time limits. By substituting Eqs. (28) and (29) into Eq. (27), and then using Eq. (30), the mathematical model for the stiffened plate is found to be

$$\delta \int_{t_1}^{t_2} \left\{ \frac{1}{2}\delta_p^T \left(\int_A N_p^T m_p N_p \, \mathrm{d}A + T_{sp}^T \int_{-1}^{1} \Lambda^T N_s^T m_s N_s \Lambda \, \mathrm{d}\zeta T_{sp} \right) \delta_p \right.$$
$$- \delta_p^T \left[\frac{1}{2} \left(\int_A B_p^T D_p B_p \, \mathrm{d}A + T_{sp}^T \int_{-1}^{1} \Lambda^T B_s^T D_s B_s \Lambda \det J \, \mathrm{d}\zeta T_{sp} \right. \right.$$
$$\left. \left. + \alpha_p \int_{\Gamma_u} N_p^T N_p \, \mathrm{d}\Gamma \right) \delta_p - \alpha_p \int_{\Gamma_u} N_p^T \bar{u} \, \mathrm{d} - \int_{\Gamma_t} N_p^T f \, \mathrm{d}\Gamma \right] \left. \right\} \mathrm{d}t = 0 \tag{31}$$

Solving Eq. (31) will result in equations of motion:

$$(M_p + M_s)\ddot{\delta}_p + (K_p + K_s)\delta_p = F \tag{32}$$

M_p, M_s, K_p, K_s, and F are defined in the Appendix. The damping matrix is assumed to be given as

$$C = a_R(M_p + M_s) + b_R(K_p + K_s) \tag{33}$$

where a_R and b_R are Rayleigh's coefficients.

III. Results and Discussion

To check the accuracy of the present meshless formulation and the behavior of the stiffened plate under various circumstances, a number of numerical examples are given. The size of the rectangular support domain is discussed in detail by Peng et al. [13,14] for buckling and free-vibration analysis of a plate with straight stiffeners in the x and y directions. It is suggested in these references that satisfactory convergence and computational cost can be achieved by using the scaling factor ($\mathrm{d}_{\max} = \mathrm{d}x_i/\mathrm{d}p$, $\mathrm{d}_{\max} = \mathrm{d}y_i/\mathrm{d}p$, and d_p: the distance between neighboring nodes) in the range of 3–4. In this paper, the rectangular support domain is considered, and the scaling factor is four in both the x and y directions. To evaluate integrations involved in stiffness and mass matrices [Eq. (A9)] over each cell, our experience suggests that 16 integration points in each cell can be sufficient to obtain accurate results with relatively less computational cost.

A. Simply Supported Plate with a Single Stiffener

Free vibration of a rectangular plate simply supported on all four edges and with one central stiffener has been considered, as shown in Fig. 9. Plate and stiffener properties are also given in this figure. Chen et al. [6] solved this problem by using the Ritz–Galerkin method with the B-spline as trial functions. In their paper, the results are compared to results given by other different researchers. However, in their study, the formulation is restricted to stiffeners that are placed in the x or y directions. Bhimaraddi et al. [4] studied the same problem by using the FEM. They used the shell element and the beam element for modeling the plate and stiffener, respectively. In their research, the effect of shear deformation and rotary inertia was taken into account.

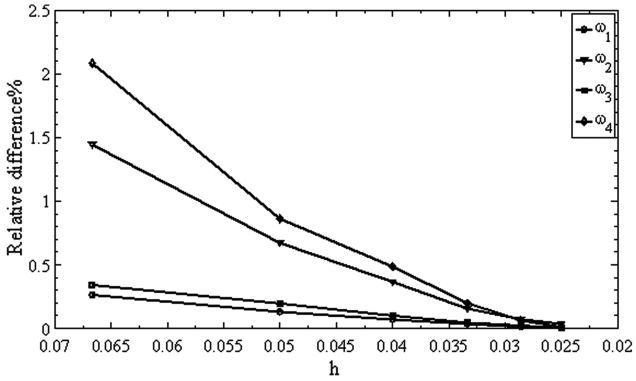

a)

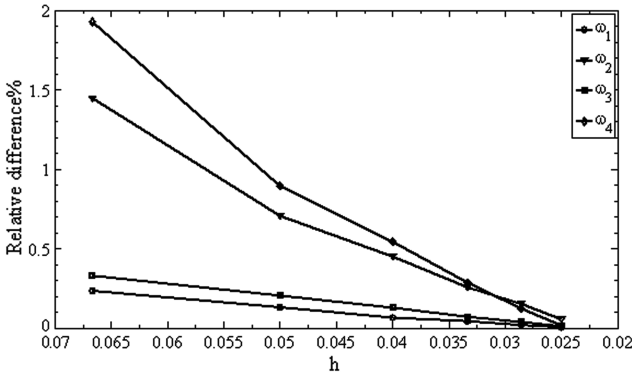

b)

Fig. 11 Relative difference in natural frequencies for the four modes: a) mesh-free and b) ANSYS.

Zeng and Bert [7] have also studied this problem. They used the DQ method for solving the problem. In addition to the mesh-free method, the problem is also modeled in ANSYS by using 600 SHELL63 elements for modeling the plate and 20 BEAM188 elements for modeling the stiffener. In the meshless code, 24×16 uniform locations are considered for modeling the plate, and 16 locations of nodes are considered for modeling the stiffener. Table 1 shows the first 10 natural frequencies. It can be seen that there is a good agreement between the results of the present mesh-free analysis, those available in the literature, and those obtained by using ANSYS. The mode shapes of the stiffened plate, which are calculated by using the present code and ANSYS, are shown in Fig. 10. The results are in good agreement.

The accuracy of the present mesh-free formulation can be evaluated by considering the convergence. In this method, it is mentioned that there is no need of matching the nodes of a stiffener and the nodes of the plate. The relative difference in the results given by this code, with respect to a mesh-free scheme with 30×20 nodes

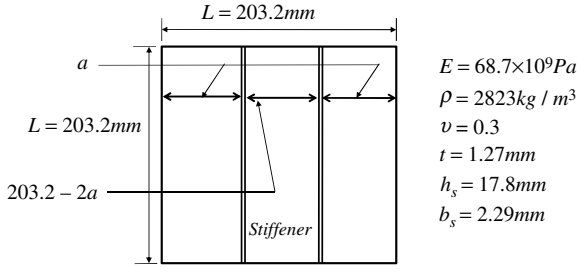

Fig. 12 Square plate with double stiffeners.

Table 2 Ten natural frequencies (Hz) for clamped plate with double stiffeners

Mode	Experimental [3]	Theoretical [3]	Ritz (B-splines) [6]	FEM [5]	FEM [4]	DQ [7]	ANSYS	Mesh-free
1	909	965	978	943	911	915	909	909
2	1204	1282	1283	1237	1198	1242	1209	1201
3	1319	1364	1371	1331	1293	1344	1296	1301
4	1506	1418	1435	1361	1400	1414	1360	1380
5	1560	1602	1592	1561	1512	——	1530	1543
6	1693	1757	1719	1706	1648	——	1680	1693
7	1807	1854	1861	1808	1763	——	1776	1795
8	1962	2015	1997	1962	1908	——	1931	1984
9	2052	2109	2055	2057	1989	——	2023	2016
10	2097	2253	2459	2163	——	——	2090	2072

for the plate and 20 nodes for the stiffeners, is calculated. Also, a convergence study for the ANSYS results has been carried out. The relative difference of the ANSYS is with respect to 30×20 nodes, and h is the distance between the two nodes in mesh free and ANSYS, respectively. As seen in Fig. 11, convergence occurred for all four natural frequencies; however, contrary to the intuition, the relative difference of the fourth natural frequency is less than the third natural frequency. By comparing two figures, it can be observed that, for the higher frequencies, mesh-free results converge faster than the FEM.

B. Plate Having Two Stiffeners and Clamped on All Sides

The double stiffeners plate with all edges clamped, analyzed by Olson and Hazell [3] theoretically and experimentally, by Chen et al. [6] using the Ritz method, by Holopainen [5] using the FEM, by Bhimaraddi et al. [4] implementing FEM by using shell and beam elements, and by Zeng and Bert [7] using DQ, is selected as the second example.

The geometry and material properties of the plate and stiffeners ($a = 67.73$ mm) are shown in Fig. 12. The first 10 natural frequencies are demonstrated in Table 2. It can be seen that the results of the

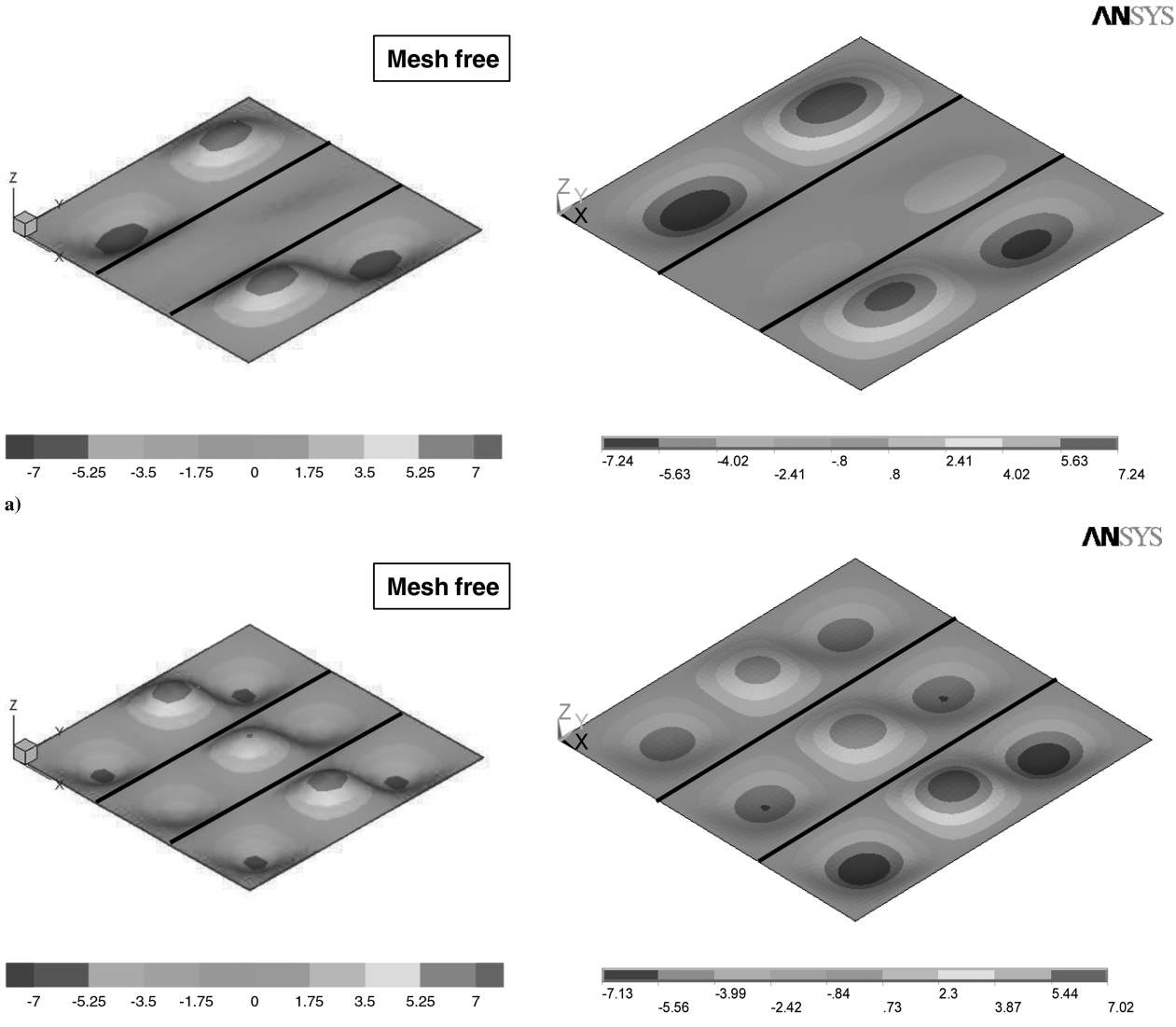

Fig. 13 Mode shapes obtained for a plate with two stiffeners, using a mesh-free method (left) and ANSYS (right): a) fifth mode shape and b) tenth mode shape.

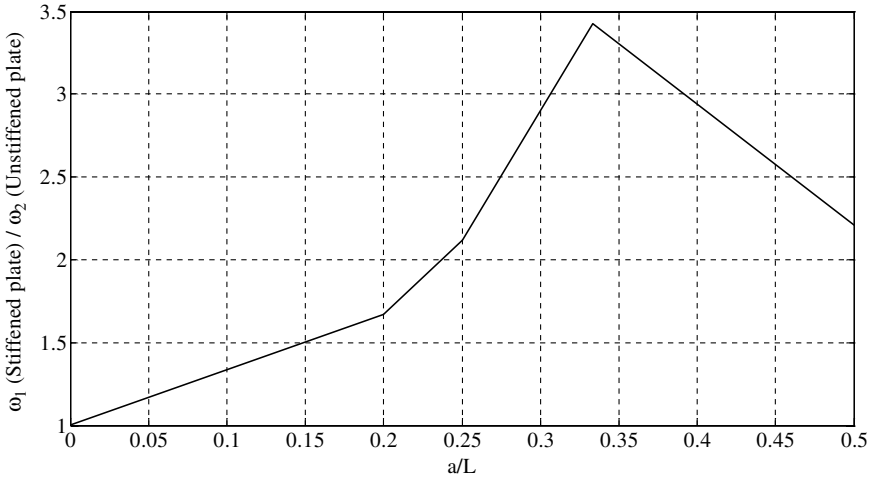

Fig. 14 Effect of stiffeners position on the natural frequency of stiffened plate.

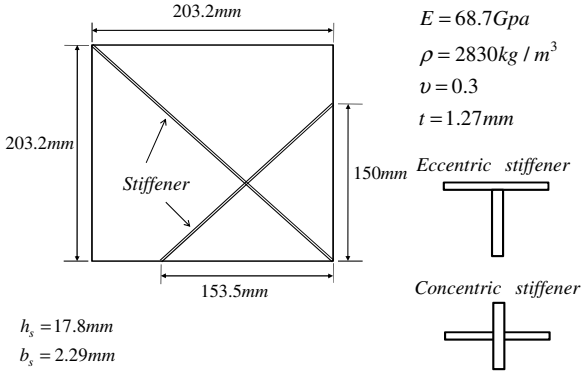

Fig. 15 Square plate with two arbitrary orientated stiffeners.

present analysis, those that can be found in the literature, and those obtained by ANSYS are close. When using ANSYS, 1225 SHELL63 elements were used for modeling the plate, and 70 BEAM188 elements were used for modeling each stiffener. For the mesh-free domain, 18 × 18 nodes were considered for the plate, and 18 nodes were considered for each stiffener. The fifth and tenth mode shapes of the stiffened plate, which are obtained by ANSYS and the developed meshless code, are shown in Fig. 13.

In Fig. 14, the effect of the location of the stiffeners is studied. It can be seen that, as the distance between the two stiffeners decreases, the ratio of natural frequency (the natural frequency of the stiffened plate to the corresponding natural frequency of the unstiffened plate) first increases and then decreases. As a simple check, one can see that, as the distance of the stiffener from the nearby edge becomes zero, the fundamental frequency of the stiffened plate approaches that of the clamped unstiffened plate.

C. Simply Supported Plate with Arbitrarily Inclined Stiffeners

To validate the applicability of the proposed EFG formulation for the analysis of plates with arbitrary orientated stiffeners, a new example is suggested. This example studies the free vibration of a simply supported plate with stiffeners placed at arbitrary orientations. Both the concentric and eccentric stiffener configurations are studied. The dimensions and material properties of the panel are presented in Fig. 15. For comparison purposes, the complete stiffened plate was modeled in ANSYS with an irregular mesh composed of 1600 SHELL63 elements for modeling the plate and 80 BEAM188 elements for modeling the stiffeners. The meshless scheme is chosen to be 18 × 18 nodes for the plate and 40 nodes for the stiffeners. It is important to note that, in ANSYS, the mesh is determined by the position and orientation of the stiffener within the plate, which limits the flexibility of the plate mesh. In Table 3, the natural frequencies for the eccentric- and concentric-inclined stiffeners are given. Also, the mode shapes can be observed in Fig. 16. As seen in Table 3, a close agreement of results, using the present formulation and ANSYS, has been achieved for all the natural frequencies. Also, by comparison of the results of eccentric and concentric inclined stiffeners, it can be concluded that, considering the eccentricity affects some modes considerably, but it does not influence some other modes very much. The reason is that, in some of the modes, the stiffener deforms only slightly. Hence, the inclusion of eccentricity does not influence these modes appreciably. This fact can be used to place the stiffeners in a way to impact modes with specific frequencies (e.g., for desired dynamic response under known excitation frequencies).

D. Simply Supported Plate with a Curvilinear Stiffener

The free-vibration analysis of a simply supported plate with a curvilinear stiffener is considered. Two stiffener configurations are considered. The geometry and the material properties are shown in Fig. 17. The natural frequencies of a plate with stiffener 1 are shown in Table 4. To check the accuracy of the present formulation, analysis has been carried out using the present formulation and also using the ANSYS software. In the mesh-free method, 18 × 18 nodes are used for the plate and 24 nodes are used for the stiffener. In the ANSYS modeling, 2120 SHELL63 elements were used for the plate and 50 BEAM188 elements were used for the curvilinear stiffener. In Table 4, a good agreement of results is observed between the ANSYS and the present EFG solution. The fifth and tenth mode shapes of the stiffened plate, which are given by the mesh-free and ANSYS, are shown in Fig. 18. It was found that the ANSYS results were all in excellent agreement with the present predictions. It is also of interest to compare the CPU time of ANSYS and the mesh-free method. As seen in Table 4, ANSYS is 20% more efficient in terms of CPU time

Table 3 Ten natural frequencies (Hz) for simply supported plate with inclined stiffeners

	Eccentric stiffeners		Concentric stiffeners	
Mode	ANSYS	Mesh-free	ANSYS	Mesh-free
1	565	561	401	409
2	577	578	562	561
3	946	951	767	770
4	1035	1037	1019	1025
5	1169	1170	1058	1057
6	1397	1371	1393	1396
7	1506	1492	1406	1400
8	1562	1530	1491	1489
9	1639	1634	1573	1564
10	1658	1656	1708	1706

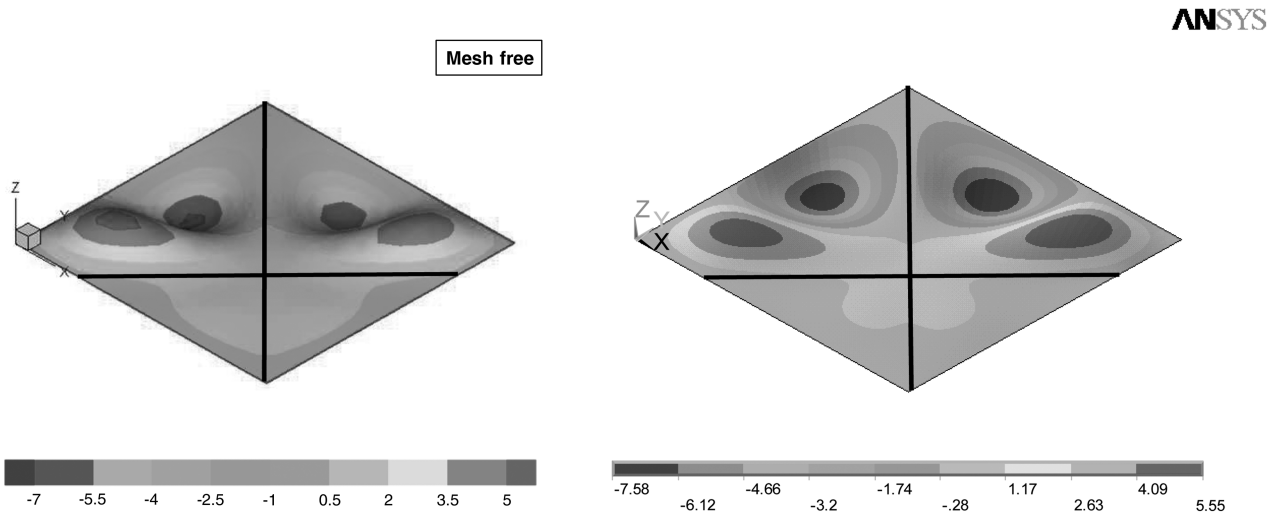

a)

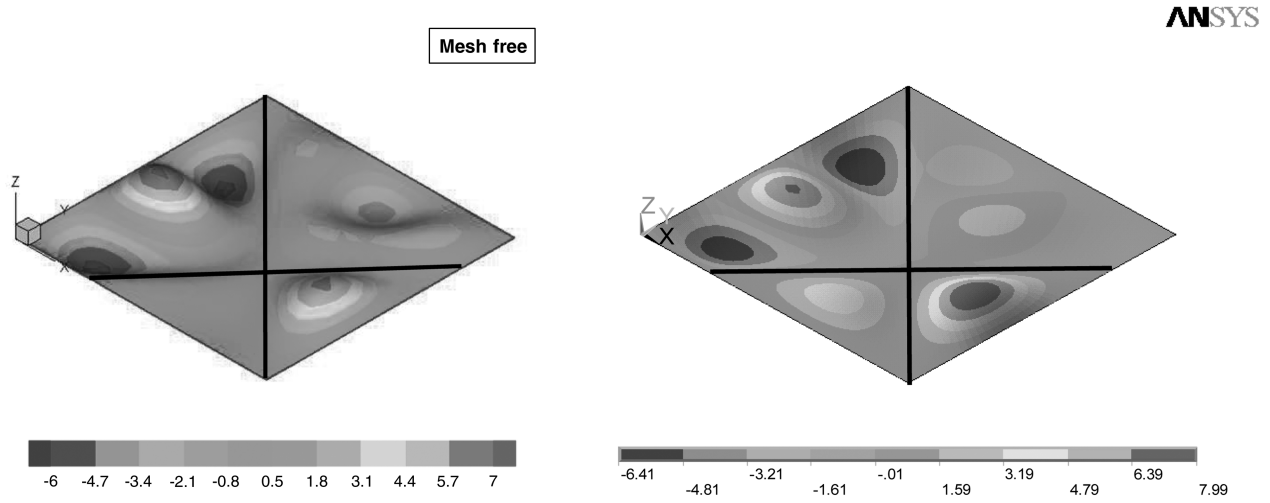

b)

Fig. 16 Mode shapes obtained for a plate with inclined stiffeners using a mesh-free method (left) and ANSYS (right): a) fifth mode shape and b) tenth mode shape.

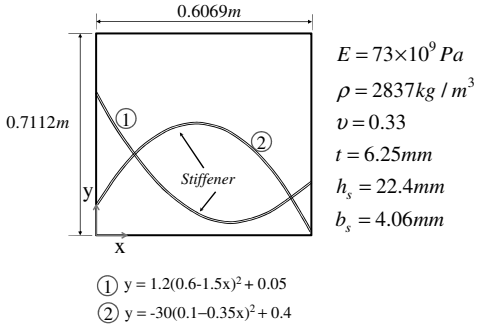

$E = 73\times10^9\ Pa$
$\rho = 2837 kg/m^3$
$\upsilon = 0.33$
$t = 6.25mm$
$h_s = 22.4mm$
$b_s = 4.06mm$

Fig. 17 Curvilinearly stiffened plate.

than the mesh-free code. However, it can be observed in Table 5, which shows the natural frequencies of a plate with stiffener 2, that, as the stiffener shape changes while the plate geometry properties are kept unchanged, the mesh-free code is 40% more efficient in terms of CPU time than ANSYS.

E. Frequency Response of a Plate with Curvilinear Stiffeners

In this section, the harmonic response of a plate with curvilinear stiffeners is considered. The geometry of the stiffeners is defined in Fig. 17. Harmonic excitation $P = |P|e^{iwt}$ ($|P| = 10$ kN/m^2) is imposed on the plate along the transverse direction to study the harmonic response. The frequency of excitation covers the first nine mode shapes. The aim is to seek the effect of curvilinear stiffeners on the harmonic response. The damping ratio for this particular example is 2%, and the mass of the plate is 7.69 kg. The mass of the curvilinear stiffener can be defined by

Table 4 Ten natural frequencies (Hz) for simply supported plate with a curvilinear stiffener (stiffener 1)

Mode	ANSYS	Mesh-free
1	84	83
2	183	175
3	213	217
4	316	319
5	347	327
6	417	421
7	485	489
8	536	521
9	567	561
10	662	661
CPU time[a]	1	1.2

[a]Time is normalized.

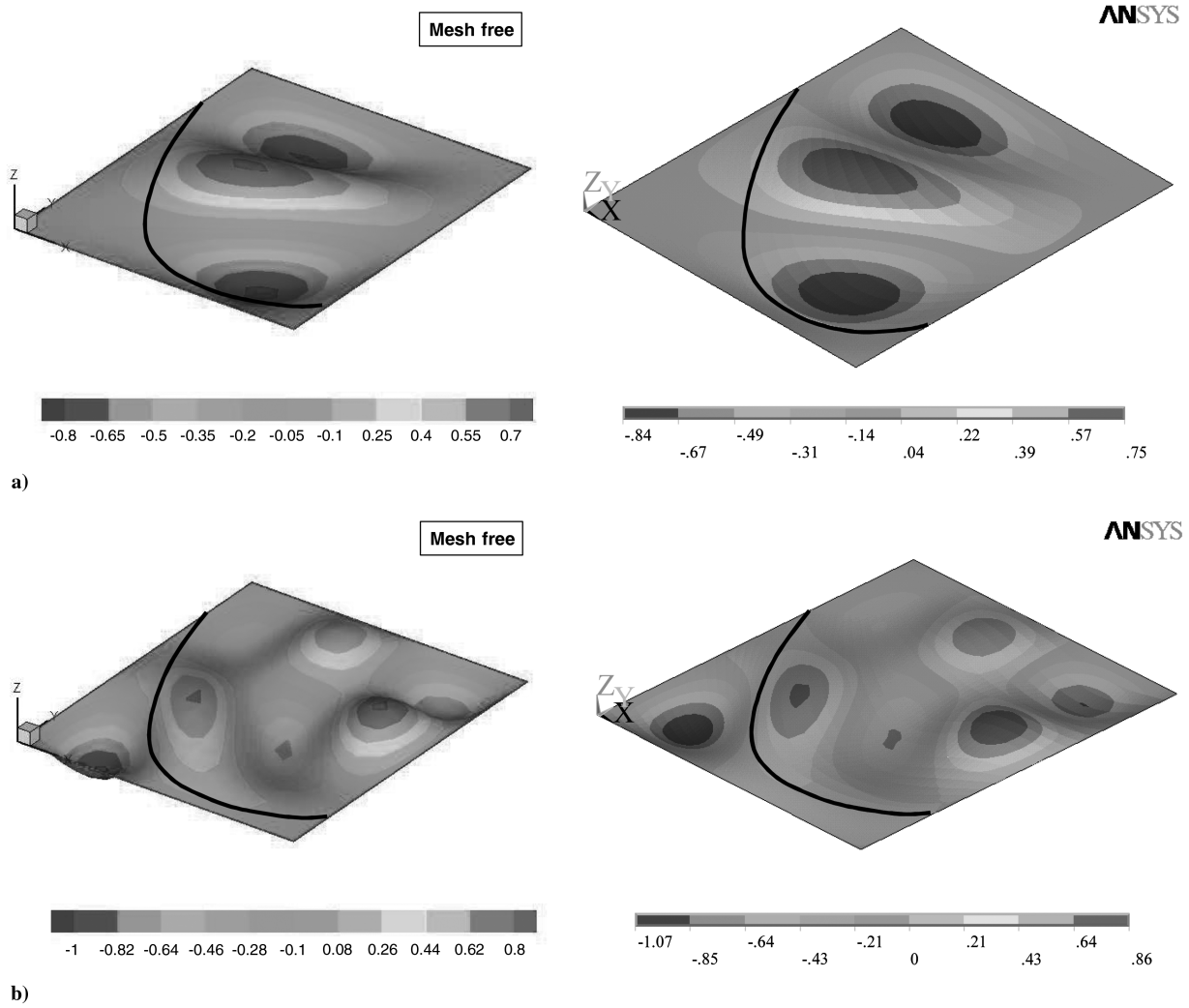

Fig. 18 Mode shapes obtained for a plate with a curvilinear stiffener using a mesh-free method (left) and ANSYS, a commercial available software (right): a) fifth mode shape and b) tenth mode shape.

$$m_s = \int_\ell \rho_s A_s \, \mathrm{d}\ell \tag{34}$$

The total mass of the plate with one stiffener and two stiffeners is 7.91 and 8.16 kg, respectively. As seen, the stiffener does not change the mass of the structure considerably. However, as seen in Fig. 19, adding stiffeners can increase the natural frequencies of structure, and it can decrease the average deflection of the stiffened plate. It can be concluded that the stiffener contributes to the stiffness matrix significantly. By using the contribution of the stiffener to the stiffness matrix, a desired level of the natural frequency and the peak of average deflection

$$w_{\text{ave}} = \sqrt{\frac{1}{n}\sum_{i=1}^{n} w_i^2}$$

(with n being the number of nodes) corresponding to a given excitation frequency can be achieved by adjusting the curvature and the location of one or more stiffeners.

Table 5 Ten natural frequencies (Hz) for simply supported plate with a curvilinear stiffener (stiffener 2)

Mode	ANSYS	Mesh-free
1	83	85
2	190	184
3	229	241
4	316	314
5	331	327
6	454	457
7	485	500
8	538	526
9	558	561
10	688	680
CPU time	1.4	1

[a]Time is normalized.

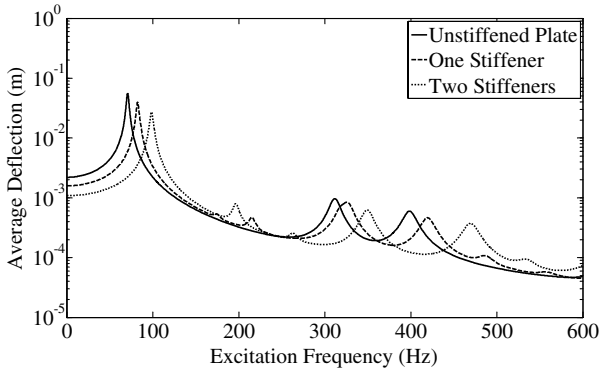

Fig. 19 Effects of the stiffener on the harmonic responses.

IV. Conclusions

In this paper, the EFG method has been successfully used for vibration analysis of the plate with straight, arbitrary oriented, as well as curvilinear, stiffeners. By employing the displacement compatibility conditions at the contact surface between the plate and the stiffener, the displacement field of the stiffener is expressed in terms of the displacements of the plate. The essential boundary conditions are imposed by using the penalty method. Numerical examples with different boundary conditions and a different stiffener location and curvature have been solved to verify the feasibility of the presented meshless method for solving the problems, and the results show that the accuracy is comparable with that of the other methods. Because there is no mesh in the meshless method to construct the shape function, the formulation allows the positioning of the stiffener anywhere within the plate, which gives a greater flexibility in the choice of the number of nodes used for both representing the plate as well as the stiffeners. This capability can be used in the topological placement of stiffeners using the EFG method by updating the stiffness and mass matrices of stiffeners while the stiffness and mass matrices of the plate are kept unchanged. This is the subject of ongoing research in our group.

Appendix: Matrices for Element-Free Galerkin Formulation

Based on the first-order shear deformation theory [16], the displacement field of a plate is expressed as

$$\begin{aligned} u_x(x,y,z,t) &= u_{p_0}(x,y,t) + z\varphi_{px}(x,y,t);\\ v_y(x,y,z,t) &= v_{p_0}(x,y,t) + z\varphi_{py}(x,y,t);\\ w_z(x,y,z,t) &= w_{p_0}(x,y,t) \end{aligned} \tag{A1}$$

where u_x, v_y, and v_y are the displacement components along the x, y, and z directions, respectively; φ_{px} and φ_{py} are the rotations with respect to the y and x axes; u_{p_0}, v_{p_0}, and w_{p_0} are the midplane displacements; and p indicates the plate (see Fig. 1). The strains associated with these displacement components are [16]

$$\varepsilon_p = \begin{Bmatrix} \varepsilon_{px}\\ \varepsilon_{py}\\ \gamma_{pxy}\\ \gamma_{pxz}\\ \gamma_{pyz}\\ \kappa_{px}\\ \kappa_{py}\\ \kappa_{pxy} \end{Bmatrix} = \begin{Bmatrix} \frac{\partial u_{p_0}}{\partial x}\\ \frac{\partial v_{p_0}}{\partial y}\\ \frac{\partial v_{p_0}}{\partial x} + \frac{\partial u_{p_0}}{\partial y}\\ \frac{\partial w_{p_0}}{\partial x} + \varphi_{px}\\ \frac{\partial w_{p_0}}{\partial y} + \varphi_{py}\\ \frac{\partial \varphi_{px}}{\partial x}\\ \frac{\partial \varphi_{py}}{\partial y}\\ \frac{\partial \varphi_{py}}{\partial x} + \frac{\partial \varphi_{px}}{\partial y} \end{Bmatrix} = \begin{bmatrix} \frac{\partial}{\partial x} & 0 & 0 & 0 & 0\\ 0 & \frac{\partial}{\partial y} & 0 & 0 & 0\\ \frac{\partial}{\partial y} & \frac{\partial}{\partial x} & 0 & 0 & 0\\ 0 & 0 & 1 & 0 & \frac{\partial}{\partial x}\\ 0 & 0 & 0 & 1 & \frac{\partial}{\partial y}\\ 0 & 0 & \frac{\partial}{\partial x} & 0 & 0\\ 0 & 0 & 0 & \frac{\partial}{\partial y} & 0\\ 0 & 0 & \frac{\partial}{\partial y} & \frac{\partial}{\partial x} & 0 \end{bmatrix} \begin{Bmatrix} u_{p_0}\\ v_{p_0}\\ \varphi_{px}\\ \varphi_{py}\\ w_{p_0} \end{Bmatrix} = L_p u_p \tag{A2}$$

The generalized plate stress–strain matrix for an isotropic material is

$$D_p = \frac{E_p h_p}{1-v^2} \begin{bmatrix} 1 & & & & & & & \\ v & 1 & & & & & & \\ 0 & 0 & \frac{1-v}{2} & & & \text{sym.} & & \\ 0 & 0 & 0 & K_G\frac{1-v}{2} & & & & \\ 0 & 0 & 0 & 0 & K_G\frac{1-v}{2} & & & \\ 0 & 0 & 0 & 0 & 0 & \frac{h_p^2}{12} & & \\ 0 & 0 & 0 & 0 & 0 & \frac{vh_p^2}{12} & \frac{h_p^2}{12} & \\ 0 & 0 & 0 & 0 & 0 & 0 & 0 & \frac{h_p^2(1-v)}{24} \end{bmatrix} \tag{A3}$$

where h_p is the thickness of the plate, A is the area of the plate, E_p is Young's modulus, υ is the Poisson's ratio, and K_G is the shear correction factor (it is taken as $K_G = \frac{5}{6}$ in this paper).

The mass matrix is

$$m_p = \rho_p \begin{bmatrix} h_p & 0 & 0 & 0 & 0\\ 0 & h_p & 0 & 0 & 0\\ 0 & 0 & \frac{h_p^3}{12} & 0 & 0\\ 0 & 0 & 0 & \frac{h_p^3}{12} & 0\\ 0 & 0 & 0 & 0 & h_p \end{bmatrix} \tag{A4}$$

where ρ_p is the density of plate material.

The B matrices for defining the strains in terms of nodal displacements are

$$[B_p]_i = \begin{bmatrix} \frac{\partial N_{pi}}{\partial x} & 0 & 0 & 0 & 0\\ 0 & \frac{\partial N_{pi}}{\partial y} & 0 & 0 & 0\\ \frac{\partial N_{pi}}{\partial y} & \frac{\partial N_{pi}}{\partial x} & 0 & 0 & 0\\ 0 & 0 & N_{pi} & 0 & \frac{\partial N_{pi}}{\partial x}\\ 0 & 0 & 0 & N_{pi} & \frac{\partial N_{pi}}{\partial y}\\ 0 & 0 & \frac{\partial N_{pi}}{\partial x} & 0 & 0\\ 0 & 0 & 0 & \frac{\partial N_{pi}}{\partial y} & 0\\ 0 & 0 & \frac{\partial N_{pi}}{\partial y} & \frac{\partial N_{pi}}{\partial x} & 0 \end{bmatrix} \tag{A5}$$

$$[B_s]_i = \begin{bmatrix} \frac{1}{\det J}\frac{\mathrm{d}N_{si}}{\mathrm{d}\zeta} & \frac{N_{si}}{R} & 0 & 0 & 0\\ -\frac{N_{si}}{R} & \frac{1}{\det J}\frac{\mathrm{d}N_{si}}{\mathrm{d}\zeta} & 0 & 0 & 0\\ 0 & 0 & N_{si} & 0 & \frac{1}{\det J}\frac{\mathrm{d}N_{si}}{\mathrm{d}\zeta}\\ 0 & 0 & \frac{1}{\det J}\frac{\mathrm{d}N_{si}}{\mathrm{d}\zeta} & \frac{N_{si}}{R} & 0\\ 0 & 0 & -\frac{N_{si}}{R} & \frac{1}{\det J}\frac{\mathrm{d}N_{si}}{\mathrm{d}\zeta} & 0 \end{bmatrix} \tag{A6}$$

The nodal displacements for the plate and the stiffener can be defined as

$$\begin{aligned} \delta_s &= [u_{s1} \;\; v_{s1} \;\; \varphi_{sx1} \;\; \varphi_{sy1} \;\; w_{s1} \;\; \ldots \;\; u_{sN} \;\; v_{sN} \;\; \varphi_{sxN} \;\; \varphi_{syN} \;\; w_{sN}]^T;\\ \delta_p &= [u_{p1} \;\; v_{p1} \;\; \varphi_{px1} \;\; \varphi_{py1} \;\; w_{p1} \;\; \ldots \;\; u_{pn} \;\; v_{pn} \;\; \varphi_{pxn} \;\; \varphi_{pyn} \;\; w_{pn}]^T \end{aligned} \tag{A7}$$

The transformation matrices can be written as

$$T_{pu} = \begin{bmatrix} N_{p1}(x_1,y_1) & N_{p2}(x_1,y_1) & \ldots & N_{pn}(x_1,y_1)\\ \vdots & \vdots & \ddots & \vdots\\ N_{p1}(x_N,y_N) & N_{p2}(x_N,y_N) & \ldots & N_{pn}(x_N,y_N) \end{bmatrix}$$

$$T_{su} = \begin{bmatrix} N_{s1}(x_1,y_1) & N_{s2}(x_1,y_1) & \ldots & N_{sN}(x_1,y_1)\\ \vdots & \vdots & \ddots & \vdots\\ N_{s1}(x_N,y_N) & N_{s2}(x_N,y_N) & \ldots & N_{sN}(x_N,y_N) \end{bmatrix} \tag{A8}$$

The other T matrices can be defined in the same way.

The stiffness and mass matrices and the force vector are

$$K_p = \int_A B_p^T D_p B_p \, dA + \alpha_p \int_{\Gamma_u} N_p^T N_p \, d\Gamma;$$

$$K_s = T_{sp}^T \int_{-1}^{1} \Lambda^T B_s^T D_s B_s \Lambda \det J \, d\zeta T_{sp};$$

$$M_p = \int_A N_p^T m_p N_p \, dA;$$

$$M_s = T_{sp}^T \int_{-1}^{1} \Lambda^T N_s^T m_s N_s \Lambda \det J \, d\zeta T_{sp};$$

$$F = \int_{\Gamma_t} N_p^T f \, d\Gamma + \alpha_p \int_{\Gamma_u} N_p^T \bar{u} \, d\Gamma \tag{A9}$$

Acknowledgments

The work presented here was funded under the NASA Subsonic Fixed Wing Hybrid Body Technologies National Research Announcement (NRA) (NASA NN L08AA02C), with Karen Taminger as the Associate Principal Investigator and Cynthina Lach as the Contract Officer Technical Representative . We are thankful to both Taminger and Lach for their suggestions. The authors would also like to thank our partners in the NRA project (Bob Olliffe, John Barnes, Elizabeth Delany, and Steve Englestad), and all of the Lockheed Martin Aeronautics Company of Marietta, Georgia for technical discussions. Additionally, the authors would like to thank the other members of the unitized structure group: Sham Gurav, Sameer Mulani, Thi Dang, Manav Bhatia, Pankaj Joshi, and Thomas McQuigg. Thanks are also due to the Institute for Critical Technologies and Applied Sciences for providing laboratory space and other infrastructure.

References

[1] Kendrick, S., "The Analysis of a Flat Plated Grillage," *European Shipbuilding*, Vol. 27, No. 5, 1956, pp. 4–10.

[2] Schade, H. A., "The Orthogonally Stiffened Plate Under Uniform Lateral Load," *Journal of Applied Mechanics*, Vol. 7, No. 4, 1940, pp. 143–146.

[3] Olson, M. D., and Hazell, C. R., "Vibration Studies of Some Integral Rib-Stiffened Plates," *Journal of Sound and Vibration*, Vol. 50, No. 1, 1977, pp. 43–61.
doi:10.1016/0022-460X(77)90550-8

[4] Bhimaraddi, A., Carr, A. J., and Moss, M. J., "Finite Element Analysis of Laminated Shells of Revolution with Laminated Stiffeners," *Computers and Structures*, Vol. 33, No. 1, 1989, pp. 295–305.
doi:10.1016/0045-7949(89)90153-3

[5] Holopainen, T. P., "Finite Element Free Vibration Analysis of Eccentrically Stiffened Plates," *Computers and Structures*, Vol. 56, No. 6, 1995, pp. 993–1007.
doi:10.1016/0045-7949(94)00574-M

[6] Chen, C. J., Liu, W., and Chern, S. M., "Vibration Analysis of Stiffened Plate," *Computers and Structures*, Vol. 50, No. 4, 1994, pp. 471–480.
doi:10.1016/0045-7949(94)90017-5

[7] Zeng, A., and Bert, C. W., "A Differential Quadrature Analysis of Vibration for Rectangular Stiffened Plates," *Journal of Sound and Vibration*, Vol. 241, No. 2, 2001, pp. 247–252.
doi:10.1006/jsvi.2000.3295

[8] Gangadhara Prusty, B., and Satsangi, S. K., "Analysis of Stiffened Shell for Ships and Ocean Structures by Finite Element Method," *Ocean Engineering*, Vol. 28, No. 6, 2001, pp. 621–638.
doi:10.1016/S0029-8018(00)00021-4

[9] Barik, M., and Mukhopadhyay, M., "A New Stiffened Plate Element for the Analysis of Arbitrary Plates," *Thin-Walled Structures*, Vol. 40, No. 7, 2002, pp. 625–639.
doi:10.1016/S0263-8231(02)00016-2

[10] Belytschko, T., Lu, Y. Y., and Gu, L., "Element-Free Galerkin Methods," *International Journal for Numerical Methods in Engineering*, Vol. 37, No. 2, 1994, pp. 229–256.
doi:10.1002/nme.1620370205

[11] Krysl, P., and Belytschko, T., "Analysis of Thin Shells by the Element Free Galerkin Method," *International Journal of Solids and Structures*, Vol. 33, No. 20, 1996, pp. 3057–3080.
doi:10.1016/0020-7683(95)00265-0

[12] Belytschko, T., Krongauz, Y., Organ, D., Fleming, M., and Krysl, P., "Meshless Methods: An Overview and Recent Developments," *Computer Methods in Applied Mechanics and Engineering*, Vol. 139, Nos. 1–4, 1996, pp. 3–47.
doi:10.1016/S0045-7825(96)01078-X

[13] Peng, L. X., Kitipornchai, S., and Liew, K. M., "Analysis of Rectangular Stiffened Plates Under Uniform Lateral Load Based on FSDT and Element-Free Galerkin Method," *International Journal of Mechanical Sciences*, Vol. 47, No. 2, 2005, pp. 251–276.
doi:10.1016/j.ijmecsci.2004.12.006

[14] Peng, L. X., Liew, K. M., and Kitipornchai, S., "Buckling and Free Vibration Analyses of Stiffened Plates Using the FSDT Meshfree Method," *Journal of Sound and Vibration*, Vol. 289, No. 3, 2006, pp. 421–449.
doi:10.1016/j.jsv.2005.02.023

[15] Bobaru, F., and Mukherjee, S., "Shape Sensitivity Analysis and Shape Optimization in Planar Elasticity Using the Element-Free Galerkin Method," *Computer Methods in Applied Mechanics and Engineering*, Vol. 190, No. 32–33, 2001, pp. 4319–4337.
doi:10.1016/S0045-7825(00)00321-2

[16] Reddy, J. N., *Mechanics of Laminated Composite Plates and Shells*, CRC Press, Boca Raton, FL, 2004.

[17] Martini, L., and Vitaliani, R., "On the Polynomial Convergent Formulation of aC^0 Isoparametric Skew Beam Element," *Computers and Structures*, Vol. 29, No. 3, 1988, pp. 437–449.
doi:10.1016/0045-7949(88)90396-3

[18] Lancaster, P., and Salkauskas, K., "Surfaces Generated by Moving Least-Squares Methods," *Mathematics of Computation*, Vol. 37, No. 155, 1981, pp. 141–158.
doi:10.2307/2007507

[19] Sadek, E. A., and Tawfik, S. A., "A Finite Element Model for the Analysis of Stiffened Laminated Plates," *Computers and Structures*, Vol. 75, No. 4, 2000, pp. 369–383.
doi:10.1016/S0045-7949(99)00094-2

[20] Zhu, T., and Atluri, S. N., "On a Modified Collocation Method and a Penalty Formulation for Enforcing the Essential Boundary Conditions in the Element Free Galerkin Method," *Computational Mechanics*, Vol. 21, No. 3, 1998, pp. 211–222.
doi:10.1007/s004660050296

N. Wereley
Associate Editor